

Measurement of the Positive Muon Anomalous Magnetic Moment to 0.20 ppm

D. P. Aguillard³³ T. Albahri³⁰ D. Allspach⁷ A. Anisenkov^{4,a} K. Badgley⁷ S. Baeßler^{35,b} I. Bailey^{17,c}
 L. Bailey²⁷ V. A. Baranov^{15,d} E. Barlas-Yucel²⁸ T. Barrett⁶ E. Barzi⁷ F. Bedeschi¹⁰ M. Berz¹⁸
 M. Bhattacharya⁷ H. P. Binney³⁶ P. Bloom¹⁹ J. Bono⁷ E. Bottalico³⁰ T. Bowcock³⁰ S. Braun³⁶
 M. Bressler³² G. Cantatore^{12,e} R. M. Carey² B. C. K. Casey⁷ D. Cauz^{26,f} R. Chakraborty²⁹ A. Chapelain⁶
 S. Chappa⁷ S. Charity³⁰ C. Chen^{23,22} M. Cheng²⁸ R. Chislett²⁷ Z. Chu^{22,g} T. E. Chupp³³ C. Claessens³⁶
 M. E. Convery⁷ S. Corrodi¹ L. Crottozzi^{10,h} J. D. Crnkovic⁷ S. Dabagov^{8,i} P. T. Debevec²⁸ S. Di Falco¹⁰
 G. Di Sciascio¹¹ B. Drendel⁷ A. Driutti^{10,h} V. N. Duginov^{15,d} M. Eads²⁰ A. Edmonds² J. Esquivel⁷
 M. Farooq³³ R. Fatemi²⁹ C. Ferrari^{10,j} M. Fertl¹⁴ A. T. Fienberg³⁶ A. Fioretti^{10,j} D. Flay³² S. B. Foster²
 H. Friedsam⁷ N. S. Froemming²⁰ C. Gabbanini^{10,j} I. Gaines⁷ M. D. Galati^{10,h} S. Ganguly⁷ A. Garcia³⁶
 J. George^{32,k} L. K. Gibbons⁶ A. Gioiosa^{25,l} K. L. Giovanetti¹³ P. Girotti¹⁰ W. Gohn²⁹ L. Goodenough⁷
 T. Gorringer²⁹ J. Grange³³ S. Grant^{1,27} F. Gray²¹ S. Haciomeroglu^{5,m} T. Halewood-Leagas³⁰ D. Hampai⁸
 F. Han²⁹ J. Hempstead³⁶ D. W. Hertzog³⁶ G. Hesketh²⁷ E. Hess¹⁰ A. Hibbert³⁰ Z. Hodge³⁶ K. W. Hong³⁵
 R. Hong^{29,1} T. Hu^{23,22} Y. Hu^{22,g} M. Iacovacci^{9,n} M. Incagli¹⁰ P. Kammel³⁶ M. Kargiantoulakis⁷
 M. Karuza^{12,o} J. Kaspar³⁶ D. Kawall³² L. Kelton²⁹ A. Keshavarzi³¹ D. S. Kessler³² K. S. Khaw^{23,22}
 Z. Khechadorian⁶ N. V. Khomutov¹⁵ B. Kiburg⁷ M. Kiburg^{7,19} O. Kim³⁴ N. Kinnaird² E. Kraegeloh³³
 V. A. Krylov¹⁵ N. A. Kuchinskiy¹⁵ K. R. Labe⁶ J. LaBounty³⁶ M. Lancaster³¹ S. Lee⁵ B. Li^{22,1,p} D. Li^{22,q}
 L. Li^{22,g} I. Logashenko^{4,a} A. Lorente Campos²⁹ Z. Lu^{22,g} A. Lucà⁷ G. Lukicov²⁷ A. Lusiani^{10,r}
 A. L. Lyon⁷ B. MacCoy³⁶ R. Madrak⁷ K. Makino¹⁸ S. Mastroianni⁹ J. P. Miller² S. Miozzi¹¹ B. Mitra³⁴
 J. P. Morgan⁷ W. M. Morse³ J. Mott^{7,2} A. Nath^{9,n} J. K. Ng^{23,22} H. Nguyen⁷ Y. Oksuzian¹ Z. Omarov^{16,5}
 R. Osofsky³⁶ S. Park⁵ G. Pauletta^{26,s} G. M. Piacentino^{25,t} R. N. Pilato³⁰ K. T. Pitts^{28,u} B. Plaster²⁹
 D. Počanić³⁵ N. Pohlman²⁰ C. C. Polly⁷ J. Price³⁰ B. Quinn³⁴ M. U. H. Qureshi¹⁴ S. Ramachandran^{1,k}
 E. Ramberg⁷ R. Reimann¹⁴ B. L. Roberts² D. L. Rubin⁶ L. Santi^{26,f} C. Schlesier^{28,v} A. Schreckenberger⁷
 Y. K. Semertzidis^{5,16} D. Shemyakin^{4,a} M. Sorbara^{11,w} D. Stöckinger²⁴ J. Stapleton⁷ D. Still⁷ C. Stoughton⁷
 D. Stratakis⁷ H. E. Swanson³⁶ G. Sweetmore³¹ D. A. Sweigart⁶ M. J. Syphers²⁰ D. A. Tarazona^{6,30,18}
 T. Teubner³⁰ A. E. Tewsley-Booth^{29,33} V. Tishchenko³ N. H. Tran^{2,x} W. Turner³⁰ E. Valetov¹⁸
 D. Vasilkova^{27,30} G. Venanzoni^{30,1} V. P. Volnykh¹⁵ T. Walton⁷ A. Weisskopf¹⁸ L. Welty-Rieger⁷ P. Winter¹
 Y. Wu¹ B. Yu³⁴ M. Yucel⁷ Y. Zeng^{23,22} and C. Zhang³⁰

(The Muon $g - 2$ Collaboration)¹Argonne National Laboratory, Lemont, Illinois, USA²Boston University, Boston, Massachusetts, USA³Brookhaven National Laboratory, Upton, New York, USA⁴Budker Institute of Nuclear Physics, Novosibirsk, Russia⁵Center for Axion and Precision Physics (CAPP)/Institute for Basic Science (IBS), Daejeon, Republic of Korea⁶Cornell University, Ithaca, New York, USA⁷Fermi National Accelerator Laboratory, Batavia, Illinois, USA⁸INFN, Laboratori Nazionali di Frascati, Frascati, Italy⁹INFN, Sezione di Napoli, Naples, Italy¹⁰INFN, Sezione di Pisa, Pisa, Italy¹¹INFN, Sezione di Roma Tor Vergata, Rome, Italy¹²INFN, Sezione di Trieste, Trieste, Italy¹³Department of Physics and Astronomy, James Madison University, Harrisonburg, Virginia, USA¹⁴Institute of Physics and Cluster of Excellence PRISMA+, Johannes Gutenberg University Mainz, Mainz, Germany¹⁵Joint Institute for Nuclear Research, Dubna, Russia¹⁶Department of Physics, Korea Advanced Institute of Science and Technology (KAIST), Daejeon, Republic of Korea¹⁷Lancaster University, Lancaster, United Kingdom¹⁸Michigan State University, East Lansing, Michigan, USA¹⁹North Central College, Naperville, Illinois, USA²⁰Northern Illinois University, DeKalb, Illinois, USA²¹Regis University, Denver, Colorado, USA

²²*School of Physics and Astronomy, Shanghai Jiao Tong University, Shanghai, China*²³*Tsung-Dao Lee Institute, Shanghai Jiao Tong University, Shanghai, China*²⁴*Institut für Kern- und Teilchenphysik, Technische Universität Dresden, Dresden, Germany*²⁵*Università del Molise, Campobasso, Italy*²⁶*Università di Udine, Udine, Italy*²⁷*Department of Physics and Astronomy, University College London, London, United Kingdom*²⁸*University of Illinois at Urbana-Champaign, Urbana, Illinois, USA*²⁹*University of Kentucky, Lexington, Kentucky, USA*³⁰*University of Liverpool, Liverpool, United Kingdom*³¹*Department of Physics and Astronomy, University of Manchester, Manchester, United Kingdom*³²*Department of Physics, University of Massachusetts, Amherst, Massachusetts, USA*³³*University of Michigan, Ann Arbor, Michigan, USA*³⁴*University of Mississippi, University, Mississippi, USA*³⁵*University of Virginia, Charlottesville, Virginia, USA*³⁶*University of Washington, Seattle, Washington, USA*

(Received 10 August 2023; accepted 5 September 2023; published 17 October 2023)

We present a new measurement of the positive muon magnetic anomaly, $a_\mu \equiv (g_\mu - 2)/2$, from the Fermilab Muon $g - 2$ Experiment using data collected in 2019 and 2020. We have analyzed more than 4 times the number of positrons from muon decay than in our previous result from 2018 data. The systematic error is reduced by more than a factor of 2 due to better running conditions, a more stable beam, and improved knowledge of the magnetic field weighted by the muon distribution, $\tilde{\omega}'_p$, and of the anomalous precession frequency corrected for beam dynamics effects, ω_a . From the ratio $\omega_a/\tilde{\omega}'_p$, together with precisely determined external parameters, we determine $a_\mu = 116\,592\,057(25) \times 10^{-11}$ (0.21 ppm). Combining this result with our previous result from the 2018 data, we obtain $a_\mu(\text{FNAL}) = 116\,592\,055(24) \times 10^{-11}$ (0.20 ppm). The new experimental world average is $a_\mu(\text{exp}) = 116\,592\,059(22) \times 10^{-11}$ (0.19 ppm), which represents a factor of 2 improvement in precision.

DOI: [10.1103/PhysRevLett.131.161802](https://doi.org/10.1103/PhysRevLett.131.161802)

Introduction.—A precise experimental measurement of the muon magnetic anomaly a_μ provides a stringent test of the Standard Model (SM) as it can be theoretically predicted with high precision. Any deviation between experiment and theory may be a sign of physics beyond the SM. We report a new measurement of a_μ using data collected in 2019 (Run-2) and 2020 (Run-3) by the Muon $g - 2$ Experiment at Fermilab. The data constitute a fourfold increase in detected positrons compared to our previous measurement (Run-1) [1–4]. Analysis and run condition improvements also lead to more than a factor of 2 reduction in the systematic uncertainties, surpassing the experiment’s design goal [5].

Our Run-1 publications describe the principle of the experiment, previous results, and experimental details [1–4]. The experiment uses 3.1 GeV/c polarized muons produced at the Fermilab Muon Campus [6]. Muons are injected into a 7.112-m radius storage ring that was moved, and

significantly upgraded, from the BNL experiment [7,8]. Two key components of the storage ring are kicker magnets that direct the injected muons onto the central orbit of the storage ring [9] and electrostatic quadrupoles (ESQs) that provide vertical focusing of the stored beam [10]. The anomalous spin precession frequency ω_a —the difference between the muon spin precession frequency and the cyclotron frequency—is measured by recording the time dependence of the number of high-energy positrons detected in a series of calorimeters located on the inner radius of the storage ring [11]. The magnetic field is mapped every few days using a trolley instrumented with nuclear magnetic resonance (NMR) probes housing petroleum jelly [12]. These probes are calibrated using a retractable water-based cylindrical probe [13]. This enables the expression of the magnetic field in terms of the precession frequency of shielded protons in a spherical sample ω'_p , for which the relation between precession frequency and magnetic field is precisely known. After weighting for the muon spatial distribution, the precession frequency is denoted $\tilde{\omega}'_p$. Changes in the field between trolley measurements are tracked using NMR probes embedded in the vacuum chamber walls above and below the muon storage volume [3]. Dedicated instrumentation is used to measure transient magnetic fields caused by the pulsing of the kickers and

Published by the American Physical Society under the terms of the [Creative Commons Attribution 4.0 International license](https://creativecommons.org/licenses/by/4.0/). Further distribution of this work must maintain attribution to the author(s) and the published article’s title, journal citation, and DOI. Funded by SCOAP³.

ESQs. The spatial distribution of the muon beam within the storage ring as a function of time since injection is inferred from positron trajectories recorded using two tracking detectors [14].

We incorporated major instrumental improvements with respect to Run-1. Resistors in the high-voltage feedthroughs for the ESQ system that were damaged in Run-1 were replaced before Run-2. This upgrade greatly improved transverse beam stability. Thermal insulation was added to the storage ring magnet before Run-2 to remove diurnal temperature variations. Increased cooling power and improved air circulation in the experimental hall installed before Run-3 reduced seasonal temperature variations. The magnitude and reliability of the kicker field were improved between Run-1 and Run-2, and again within Run-3. Because of these improvements, the data are analyzed in three sets—Run-2, Run-3a, and Run-3b. A full description of the hardware upgrades, operating conditions, and analysis details will be provided in an in-depth paper currently in preparation.

The data are blinded by hiding the true value of the calorimeter digitization clock frequency. This blinding factor is different for Run-2 and Run-3.

We obtain the muon magnetic anomaly from Ref. [15],

$$a_\mu = \frac{\omega_a}{\tilde{\omega}'_p(T_r)} \frac{\mu'_p(T_r)}{\mu_e(H)} \frac{\mu_e(H)}{\mu_e} \frac{m_\mu g_e}{m_e 2}, \quad (1)$$

where this experiment measures two frequencies to form the ratio $\mathcal{R}'_\mu = \omega_a/\tilde{\omega}'_p(T_r)$, where $T_r = 34.7^\circ\text{C}$ is the temperature at which the shielded proton-to-electron magnetic moment is measured [16]. The ratio of the measured frequencies must be corrected for a number of effects, which shift the value of \mathcal{R}'_μ by +622 ppb in total. We write the ratio in terms of measured quantities and corrections as

$$\mathcal{R}'_\mu \approx \frac{f_{\text{clock}} \cdot \omega_a^m (1 + C_e + C_p + C_{pa} + C_{dd} + C_{ml})}{f_{\text{calib}} \cdot \langle \omega'_p(\vec{r}) \times M(\vec{r}) \rangle (1 + B_q + B_k)}. \quad (2)$$

The numerator consists of the clock-blinding factor f_{clock} , the measured precession frequency ω_a^m , and five corrections C_i associated with the spatial and temporal motion of the beam. In the denominator, we separate $\tilde{\omega}'_p(T_r)$ into the absolute NMR calibration procedure (indicated by f_{calib}) and the magnetic field maps, which are weighted by the muon spatial distribution and positron count [$\langle \omega'_p(\vec{r}) \times M(\vec{r}) \rangle$, where the average is over all points \vec{r} within the storage region]. We apply corrections B_i to the magnetic field to account for two fast magnetic transient fields that are synchronized to the muon storage period. The uncertainties and correction values for the elements of Eq. (2) are shown in Table I.

Anomalous precession frequency ω_a^m .—The time dependence of the number of positrons from muon decays recorded by calorimeters in a storage period is given by

TABLE I. Values and uncertainties of the \mathcal{R}'_μ terms in Eq. (2), and uncertainties due to the external parameters in Eq. (1) for a_μ . Positive C_i increases a_μ ; positive B_i decreases a_μ [see Eq. (2)]. The ω_a^m uncertainties are decomposed into statistical and systematic contributions. All values are computed with full precision and then rounded to the reported digits.

| Quantity | Correction (ppb) | Uncertainty (ppb) |
|---|------------------|-------------------|
| ω_a^m (statistical) | ... | 201 |
| ω_a^m (systematic) | ... | 25 |
| C_e | 451 | 32 |
| C_p | 170 | 10 |
| C_{pa} | -27 | 13 |
| C_{dd} | -15 | 17 |
| C_{ml} | 0 | 3 |
| $f_{\text{calib}} \cdot \langle \omega'_p(\vec{r}) \times M(\vec{r}) \rangle$ | ... | 46 |
| B_k | -21 | 13 |
| B_q | -21 | 20 |
| $\mu'_p(34.7^\circ)/\mu_e$ | ... | 11 |
| m_μ/m_e | ... | 22 |
| $g_e/2$ | ... | 0 |
| Total systematic for \mathcal{R}'_μ | ... | 70 |
| Total external parameters | ... | 25 |
| Total for a_μ | 622 | 215 |

$$N(t) = N_0 \eta_N(t) e^{-t/\gamma\tau_\mu} \times \{1 + A \eta_A(t) \cos[\omega_a^m t + \varphi_0 + \eta_\phi(t)]\}, \quad (3)$$

where N_0 is the normalization, $\gamma\tau_\mu$ is the time-dilated muon lifetime ($\approx 64.4 \mu\text{s}$), A is the average weak-decay asymmetry, and φ_0 is the average phase difference between the muon momentum and spin directions at the time of muon injection. The normalization, asymmetry, and phase have time-dependent correction factors, η_N , η_A , and η_ϕ , that account for horizontal (x) and vertical (y) beam oscillations, including x - y coupling.

Nearly all parameters in Eq. (3) have some energy dependence, but it is particularly strong for N_0 and A . We choose to combine the data in the statistically optimal way of weighting each positron by its energy-dependent asymmetry [21].

Seven different analysis groups perform independent extractions of ω_a^m by a χ^2 minimization. Each analysis team adds an independent blind offset to their result in addition to the aforementioned clock blinding. Two groups perform a new asymmetry-weighted ratio method by subdividing the data and constructing a ratio that preserves statistical power whilst reducing sensitivity to slow rate changes [2]. Each fit models the data well, producing reduced χ^2 values consistent with unity. Fourier transforms of the fit residuals have no unexpected frequencies, as shown in Fig. 1. Scans of fit start and end times, positron energy, and individual calorimeter stations show variation in ω_a^m consistent with

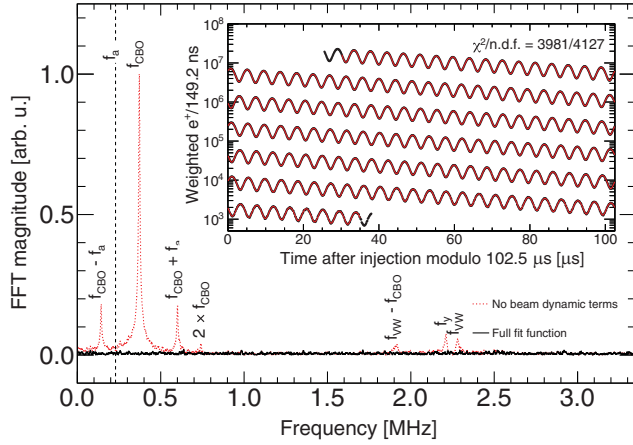


FIG. 1. Fourier transform of the residuals from a fit following Eq. (3) excluding η_N , η_A , and η_ϕ (red dashed line), and from the full fit (black line). The peaks correspond to the missing betatron frequencies and muon losses. Data are from the Run-3a data set. Inset: corresponding asymmetry-weighted e^+ time spectrum (black line) with the full fit function (red line) overlaid.

statistical expectations. After unblinding, the analysis groups determine consistent values for ω_a^m and their independently estimated systematic uncertainties. We combine the six asymmetry-weighted methods equally for the final central value and verify the result with other less sensitive methods.

The extraction of ω_a^m is the only aspect of the result with significant statistical uncertainty. The number of positrons above 1000 MeV entering the asymmetry-weighted analyses increased from 15×10^9 in Run-1 to 71×10^9 in Run-2/3. This reduces the statistical uncertainty from 434 ppb to 201 ppb.

The systematic uncertainty on ω_a^m is also reduced by a factor greater than 2 to 25 ppb. The largest reduction comes from our treatment of pileup, when two positrons enter a calorimeter close in time and are not separated by reconstruction algorithms. The difference in phase between two lower-energy positrons and a single higher-energy positron, coupled with a rate change over the storage period, can bias ω_a^m . Each calorimeter comprises a 9×6 array of PbF_2 crystals that are read out independently. Improved clustering of crystal hits in the reconstruction algorithms reduces the number of unresolved pileup events. In addition, some groups adopted a method of overlaying waveforms rather than modeling the reconstruction response to proximate crystal hits. The pileup uncertainty is reduced from 35 ppb in Run-1 to 7 ppb in Run-2/3.

The other significant reduction is related to transverse beam oscillations. The repair of the damaged ESQ resistors removes the majority of systematic effects associated with large changes in the betatron frequencies over a muon storage period. Additionally, the higher statistical precision allows for improved empirical modeling of the decoherence envelope, enabling a wider range of possibilities to be studied. The

uncertainty drops from 38 ppb in Run-1 to 21 ppb but remains the dominant systematic uncertainty for Run-2/3 for ω_a^m .

Smaller reductions are achieved in the systematic uncertainties from a residual early-to-late effect and the calorimeter gain correction (see Ref. [2]), resulting in values of 10 ppb and 5 ppb, respectively.

Beam-dynamics corrections C_i .—Five corrections must be made to convert the measured frequency ω_a^m into the anomalous precession frequency ω_a in Eq. (1).

The largest correction is due to the electric fields of the ESQs. The effect on ω_a is minimized by the choice of nominal muon momentum 3.1 GeV/c [10]. The electric field correction C_e is required to account for the momentum spread of the muon beam.

The muon momentum distribution is determined from the frequency distribution and debunching rate of the injected beam using calorimeter data. Additionally, the radial distribution of stored muons over a betatron period is obtained from tracker data. The debunching analysis takes into account differences in momentum spread along the injected bunch length that were not included in the Run-1 analysis. Accounting for this difference and using complementary tracker information reduces the C_e uncertainty from 52 ppb in Run-1 to 32 ppb in Run-2/3.

A pitch correction C_p accounts for the reduction of ω_a caused by vertical betatron oscillations. We use tracker data to extract the distribution of vertical betatron amplitudes. The analysis is largely unchanged from Run-1.

Any temporal change to the muon ensemble-average phase φ_0 in Eq. (3) will bias ω_a^m . Correlations between the muon decay position and φ_0 are accounted for through the phase acceptance correction C_{pa} . This correction is evaluated by measuring the transverse beam distribution throughout the storage period and using simulations to determine the shifts in average phase at the calorimeters. The size of C_{pa} is determined by variation in the beam spatial distribution, which is significantly reduced by replacing the damaged ESQ resistors, and the associated systematic uncertainty is reduced from 75 ppb to 13 ppb.

Phase is also correlated with muon momentum owing to the momentum-dependent phase advance in upstream beamline components [4]. A differential decay correction C_{dd} is required since the higher-momentum muons have a longer boosted lifetime than lower-momentum muons. Three separate contributions to the C_{dd} correction yield a -15 ppb correction with 17 ppb uncertainty. This correction was not applied to the Run-1 analysis.

Muons lost during a storage period can also lead to a change in the muon momentum distribution. This effect has also been greatly reduced by replacing the ESQ resistors. The correction factor C_{ml} is evaluated as 0 ± 3 ppb compared to a correction in Run-1 of -11 ± 5 ppb.

Muon-weighted magnetic field $f_{\text{calib}} \cdot \langle \omega_p' \times M \rangle$.—The increased temperature stability in Run-2 and Run-3 due to thermal magnet insulation and improved hall temperature

stability results in a significantly more stable magnetic field (RMS of 2 ppm for Run-2 and 0.5 ppm for Run-3). Additional systematic measurements of the temperature dependence of the petroleum-jelly-based NMR probes used in the trolley have reduced the systematic uncertainty from trolley temperature changes to 9–15 ppb, depending on the data set.

The calibration procedure is improved for Run-2/3 compared to Run-1. Not only are two calibrations performed, one for each run, but the process is also optimized, resulting in reduced uncertainties. Small differences between the sample volume in the calibration and the trolley probes are now corrected. In addition, correction terms for the calibration probe are determined more precisely. The overall systematic uncertainty from calibration is below 20 ppb.

As in Run-1, the magnetic field is parametrized in a multipole expansion in transverse planes. In the current analysis, the number of terms used increases from 9 to 12, improving the fit quality. The dominant uncertainties for the spatial field maps—each approximately 20 ppb in magnitude—arise from NMR frequency extraction [22], the motion effects of the trolley, and the estimated perturbation by the mechanism used to retract the trolley from the storage region.

The systematic uncertainty of tracking the field in time using the fixed probe data between two field maps is estimated by a Brownian bridge model tuned to the observed mismatch from propagating one map to another. Because of the larger number of field maps (69 in Run-2/3, compared to 14 in Run-1), the uncertainty from the field tracking is reduced to 10–16 ppb depending on the data set. We discovered and corrected a tracking bias as a function of time after the last magnet ramp-up (3–10 ppb).

The muon weighting follows the same approach used in Run-1. The more uniform field reduces the uncertainties by around a factor of 2 to 7–13 ppb. The beam distribution and azimuthally averaged magnetic field from Run-3b are shown in Fig. 2.

Magnetic field transients B_i .—Transient magnetic fields synchronized with beam injection are caused by the pulsing of ESQs and eddy currents in the kickers. Both effects require corrections to the muon-weighted magnetic field and are improved significantly compared to Run-1 by additional measurements.

In Run-1, the correction from the magnetic field transient due to vibrations caused by ESQ pulsing, B_q , was only measured at a limited number of locations around the ring. Using the same vacuum-sealed petroleum-jelly-based NMR probe, but now on a nonconductive movable device, we mapped the transient fields in the storage region between the ESQ plates azimuthally. This mapping, in combination with improved methodology and repeated measurements over time, leads to a reduction of the formerly dominant systematic effect by more than a factor of 4 to 20 ppb.

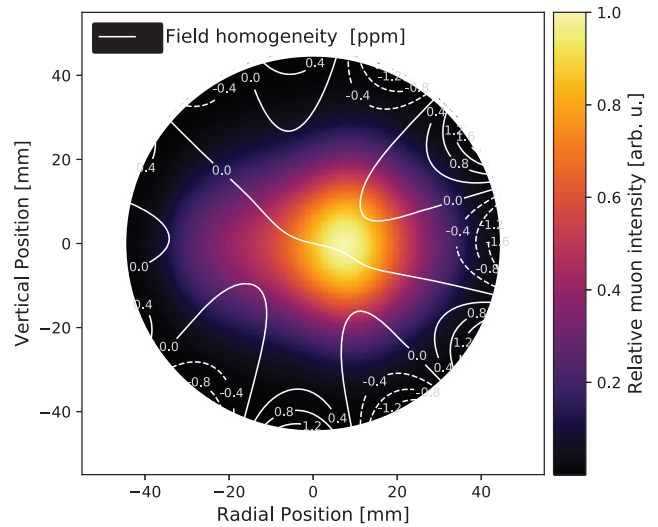


FIG. 2. Azimuthally averaged magnetic field contours overlaid on the time- and azimuthally averaged muon distribution for the Run-3b data set. The field is more uniform, and the increased kicker strength moves the beam closer to the center than in Run-1.

The effect of kicker-induced eddy currents B_k was measured with the same fiber magnetometer based on Faraday rotation in terbium gallium garnet crystals used in Run-1 [3]. An improved setup, mainly to further reduce vibrations, and more extensive measurements, reduces the uncertainty by around a factor of 3 to 13 ppb.

Consistency checks.—In addition to the three data subsets described here, the data are further subdivided based on a number of monitored experimental parameters to examine possible correlations. These parameters include ring temperature, magnet current, vacuum pressure, day/night, time since magnet ramp-up, and variables associated with the beam motion. We find no statistically significant correlations between our results and any of these parameters.

Calculation of a_μ .—Table II contains the values of ω_a and $\tilde{\omega}'_p$, including all correction terms in Eq. (2), for the three data subsets and their ratios \mathcal{R}'_μ . The statistical uncertainty dominates in each subset, and as such, the \mathcal{R}'_μ values are largely uncorrelated. Nearly all systematic

TABLE II. Measurements of ω_a , $\tilde{\omega}'_p$, and their ratios \mathcal{R}'_μ multiplied by 1000. The Run-1 value has been updated from [1] as described in the text.

| Run | $\omega_a/2\pi$ [Hz] | $\tilde{\omega}'_p/2\pi$ [Hz] | $\mathcal{R}'_\mu \times 1000$ |
|-----------|----------------------|-------------------------------|--------------------------------|
| Run-1 | | | 3.7073004(17) |
| Run-2 | 229077.408(79) | 61790875.0(3.3) | 3.7073016(13) |
| Run-3a | 229077.591(68) | 61790957.5(3.3) | 3.7072996(11) |
| Run-3b | 229077.81(11) | 61790962.3(3.3) | 3.7073029(18) |
| Run-2/3 | | | 3.70730088(79) |
| Run-1/2/3 | | | 3.70730082(75) |

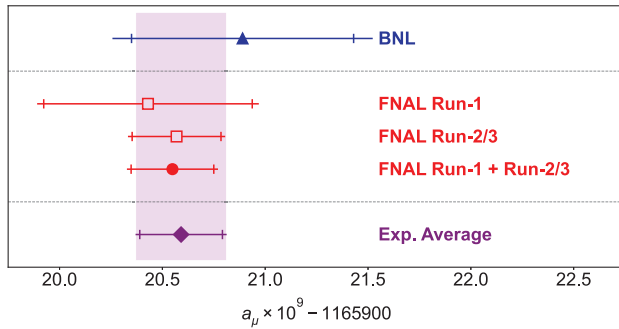


FIG. 3. Experimental values of a_μ from BNL E821 [8], our Run-1 result [1], this measurement, the combined Fermilab result, and the new experimental average. The inner tick marks indicate the statistical contribution to the total uncertainties.

uncertainties that enter into \mathcal{R}'_μ are fully correlated across the subsets. Over the course of this analysis, three small errors in the Run-1 analysis were identified [23]. The total shift in the previous result due to these errors is +28 ppb, which has been applied to the value reported in this Letter.

The weighted-average value of the Run-2/3 data is $\mathcal{R}'_\mu(\text{Run-2/3}) = 0.00370730088(75)(26)$, where the first error is statistical and the second is systematic. This value is in excellent agreement with the adjusted Run-1 value $\mathcal{R}'_\mu(\text{Run-1}) = 0.0037073004(16)(6)$. Assuming that the systematic errors are fully correlated between $\mathcal{R}'_\mu(\text{Run-2/3})$ and $\mathcal{R}'_\mu(\text{Run-1})$, we obtain the combined value of $\mathcal{R}'_\mu(\text{Run-1/2/3}) = 0.00370730082(68)(31)$.

From Eq. (1), we arrive at a new determination of the muon anomaly,

$$a_\mu(\text{FNAL}) = 116592055(24) \times 10^{-11} \quad (0.20 \text{ ppm}),$$

where the statistical, systematic, and external parameter uncertainties from Table I are combined in quadrature. The combined (BNL and FNAL) experimental (exp) average becomes

$$a_\mu(\text{exp}) = 116592059(22) \times 10^{-11} \quad (0.19 \text{ ppm}).$$

The results are displayed in Fig. 3.

A comprehensive prediction for the SM value of the muon magnetic anomaly was compiled most recently by the Muon $g - 2$ Theory Initiative in 2020 [24], using results from Refs. [25–44]. The leading-order hadronic contribution, known as hadronic vacuum polarization (HVP), was taken from $e^+e^- \rightarrow \text{hadrons}$ cross-section measurements performed by multiple experiments. However, a recent lattice calculation of HVP by the BMW Collaboration [45] shows significant tension with the e^+e^- data. In addition, a new preliminary measurement of the $e^+e^- \rightarrow \pi^+\pi^-$ cross section from the CMD-3 experiment [46] disagrees significantly with all other e^+e^- data. There are ongoing efforts to clarify the current theoretical situation [47]. While a comparison between the Fermilab result from Run-1/2/3

presented here, $a_\mu(\text{FNAL})$, and the 2020 prediction yields a discrepancy of 5.0σ , an updated prediction considering all available data will likely yield a smaller and less significant discrepancy.

In summary, we report a measurement of the muon magnetic anomaly to 0.20 ppm precision using our first three years of data. This is the most precise determination of this quantity, and it improves on our previous result by more than a factor of 2. Analysis of the remaining data from three additional years of data collection is underway and is expected to lead to another factor of 2 improvement in statistical precision.

We thank the Fermilab management and staff for their strong support of this experiment, as well as our university and national laboratory engineers, technicians, and workshops for their tremendous support. Greg Bock and Joe Lykken set the blinding clock and diligently monitored its stability. The Muon $g - 2$ Experiment was performed at the Fermi National Accelerator Laboratory, a U.S. Department of Energy, Office of Science, HEP User Facility. Fermilab is managed by Fermi Research Alliance, LLC (FRA), acting under Contract No. DE-AC02-07CH11359. Additional support for the experiment was provided by the Department of Energy offices of HEP and NP (USA), the National Science Foundation (USA), the Istituto Nazionale di Fisica Nucleare (Italy), the Science and Technology Facilities Council (UK), the Royal Society (UK), the National Natural Science Foundation of China (Grants No. 11975153 and No. 12075151), MSIP, NRF, and IBS-R017-D1 (Republic of Korea), the German Research Foundation (DFG) through the Cluster of Excellence PRISMA+ (EXC 2118/1, Project ID 39083149), the European Union Horizon 2020 research and innovation programme under the Marie Skłodowska-Curie Grant Agreements No. 101006726 and No. 734303, the European Union STRONG 2020 project under Grant Agreement No. 824093, and the Leverhulme Trust, LIP-2021-01.

^aAlso at Novosibirsk State University.

^bAlso at Oak Ridge National Laboratory.

^cAlso at The Cockcroft Institute of Accelerator Science and Technology, Daresbury, United Kingdom.

^dDeceased.

^eAlso at Università di Trieste, Trieste, Italy.

^fAlso at INFN Gruppo Collegato di Udine, Sezione di Trieste, Udine, Italy.

^gAlso at Shanghai Key Laboratory for Particle Physics and Cosmology; also at Key Lab for Particle Physics, Astrophysics and Cosmology (MOE).

^hAlso at Università di Pisa, Pisa, Italy.

ⁱAlso at Lebedev Physical Institute and NRNU MEPhI.

^jAlso at Istituto Nazionale di Ottica—Consiglio Nazionale delle Ricerche, Pisa, Italy.

^kNow at Alliance University, Bangalore, India.

^lAlso at INFN, Sezione di Pisa, Pisa, Italy.

- ^mAlso at Istinye University, Istanbul, Türkiye.
- ⁿAlso at Università di Napoli, Naples, Italy.
- ^oAlso at University of Rijeka, Rijeka, Croatia.
- ^pAlso at Research Center for Graph Computing, Zhejiang Lab, Hangzhou, Zhejiang, China.
- ^qAlso at Shenzhen Technology University, Shenzhen, Guangdong, China.
- ^rAlso at Scuola Normale Superiore, Pisa, Italy.
- ^sAlso at INFN Gruppo Collegato di Udine, Sezione di Trieste, Udine, Italy; Deceased.
- ^tAlso at INFN, Sezione di Roma Tor Vergata, Rome, Italy.
- ^uNow at Virginia Tech, Blacksburg, Virginia, USA.
- ^vNow at Wellesley College, Wellesley, Massachusetts, USA.
- ^wAlso at Università di Roma Tor Vergata, Rome, Italy.
- ^xNow at Institute for Interdisciplinary Research in Science and Education (ICISE), Quy Nhon, Binh Dinh, Vietnam.
- [1] B. Abi *et al.* (Muon $g-2$ Collaboration), Measurement of the Positive Muon Anomalous Magnetic Moment to 0.46 ppm, *Phys. Rev. Lett.* **126**, 141801 (2021).
- [2] T. Albahri *et al.* (Muon $g-2$ Collaboration), Measurement of the anomalous precession frequency of the muon in the Fermilab Muon $g-2$ Experiment, *Phys. Rev. D* **103**, 072002 (2021).
- [3] T. Albahri *et al.* (Muon $g-2$ Collaboration), Magnetic-field measurement and analysis for the Muon $g-2$ Experiment at Fermilab, *Phys. Rev. A* **103**, 042208 (2021).
- [4] T. Albahri *et al.* (Muon $g-2$ Collaboration), Beam dynamics corrections to the Run-1 measurement of the muon anomalous magnetic moment at Fermilab, *Phys. Rev. Accel. Beams* **24**, 044002 (2021).
- [5] J. Grange *et al.* (Muon $g-2$ Collaboration), Muon $g-2$ Technical Design Report, arXiv:1501.06858 .
- [6] D. Stratakis, B. Drendel, J. P. Morgan, M. J. Syphers, and N. S. Froemming, Commissioning and first results of the Fermilab Muon Campus, *Phys. Rev. Accel. Beams* **22**, 011001 (2019).
- [7] G. T. Danby *et al.*, The Brookhaven muon storage ring magnet, *Nucl. Instrum. Methods Phys. Res., Sect. A* **457**, 151 (2001).
- [8] G. W. Bennett *et al.* (Muon $g-2$ Collaboration), Final report of the muon E821 anomalous magnetic moment measurement at BNL, *Phys. Rev. D* **73**, 072003 (2006).
- [9] A. P. Schreckenberger *et al.*, The fast non-ferric kicker system for the Muon $g-2$ Experiment at Fermilab, *Nucl. Instrum. Methods Phys. Res., Sect. A* **1011**, 165597 (2021).
- [10] Y. K. Semertzidis *et al.*, The Brookhaven muon ($g-2$) storage ring high voltage quadrupoles, *Nucl. Instrum. Methods Phys. Res., Sect. A* **503**, 458 (2003).
- [11] K. S. Khaw *et al.*, Performance of the Muon $g-2$ calorimeter and readout systems measured with test beam data, *Nucl. Instrum. Methods Phys. Res., Sect. A* **945**, 162558 (2019).
- [12] S. Corrodi, P. D. Lurgio, D. Flay, J. Grange, R. Hong, D. Kawall, M. Oberling, S. Ramachandran, and P. Winter, Design and performance of an in-vacuum, magnetic field mapping system for the Muon $g-2$ Experiment, *J. Instrum.* **15**, P11008 (2020).
- [13] D. Flay *et al.*, High-accuracy absolute magnetometry with application to the Fermilab Muon $g-2$ Experiment, *J. Instrum.* **16**, P12041 (2021).
- [14] B. T. King *et al.*, The straw tracking detector for the Fermilab Muon $g-2$ Experiment, *J. Instrum.* **17**, P02035 (2022).
- [15] We use the shielded proton-to-electron magnetic moment ratio [16] and the electron g -factor [17,18] measurement. The CODATA-2018 result is used for the muon-to-electron mass ratio [19], which is determined from bound-state QED theory and measurements described in Ref. [20]. The QED factor $\mu_e(H)/\mu_e$ is computed by theory with negligible uncertainty [19].
- [16] W. D. Phillips, W. E. Cooke, and D. Kleppner, Magnetic moment of the proton in H₂O in Bohr magnetons, *Metrologia* **13**, 179 (1977).
- [17] X. Fan, T. G. Myers, B. A. D. Sukra, and G. Gabrielse, Measurement of the Electron Magnetic Moment, *Phys. Rev. Lett.* **130**, 071801 (2023).
- [18] R. L. Workman *et al.* (Particle Data Group), Review of particle physics, *Prog. Theor. Exp. Phys.* **2022**, 083C01 (2022), and 2023 update.
- [19] E. Tiesinga, P. J. Mohr, D. B. Newell, and B. N. Taylor, The 2018 CODATA recommended values of the fundamental physical constants (Web Version 8.1), <http://physics.nist.gov/constants> (2018).
- [20] W. Liu *et al.*, High Precision Measurements of the Ground State Hyperfine Structure Interval of Muonium and of the Muon Magnetic Moment, *Phys. Rev. Lett.* **82**, 711 (1999).
- [21] G. W. Bennett *et al.* (Muon $g-2$ Collaboration), Statistical equations and methods applied to the precision Muon $g-2$ Experiment at BNL, *Nucl. Instrum. Methods Phys. Res., Sect. A* **579**, 1096 (2007).
- [22] R. Hong *et al.*, Systematic and statistical uncertainties of the Hilbert-transform based high-precision FID frequency extraction method, *J. Magn. Reson.* **329**, 107020 (2021).
- [23] We have updated the Run-1 measurement with three corrections. The E-field correction C_e was inadvertently calculated using the blinded clock frequency. We have updated this to use the unblinded clock frequency. This changes the Run-1 result by +19 ppb. The phase acceptance correction C_{pa} for Run-1b was inadvertently swapped with the C_{pa} for Run-1c. We have applied these correctly now. This changes the Run-1 result by +6 ppb. A correction was applied to the temperature dependence of the magnetic susceptibility of a spherical water probe. The applied correction did not include an additional term that accounts for the temperature dependence of the density of water. We have now included this term. This changes the Run-1 result by +2 ppb. These corrections are all positive and sum to a +28 ppb correction to the Run-1 result.
- [24] T. Aoyama *et al.*, The anomalous magnetic moment of the muon in the Standard Model, *Phys. Rep.* **887**, 1 (2020).
- [25] T. Aoyama, M. Hayakawa, T. Kinoshita, and M. Nio, Complete Tenth-Order QED Contribution to the Muon $g-2$, *Phys. Rev. Lett.* **109**, 111808 (2012).
- [26] T. Aoyama, T. Kinoshita, and M. Nio, Theory of the anomalous magnetic moment of the electron, *Atoms* **7**, 28 (2019).
- [27] A. Czarnecki, W. J. Marciano, and A. Vainshtein, Refinements in electroweak contributions to the muon anomalous magnetic moment, *Phys. Rev. D* **67**, 073006 (2003); **73**, 119901(E) (2006).

- [28] C. Gneidiger, D. Stöckinger, and H. Stöckinger-Kim, The electroweak contributions to $(g-2)_\mu$ after the Higgs boson mass measurement, *Phys. Rev. D* **88**, 053005 (2013).
- [29] M. Davier, A. Hoecker, B. Malaescu, and Z. Zhang, Reevaluation of the hadronic vacuum polarisation contributions to the Standard Model predictions of the muon $g-2$ and $\alpha(m_Z^2)$ using newest hadronic cross-section data, *Eur. Phys. J. C* **77**, 827 (2017).
- [30] A. Keshavarzi, D. Nomura, and T. Teubner, Muon $g-2$ and $\alpha(M_Z^2)$: A new data-based analysis, *Phys. Rev. D* **97**, 114025 (2018).
- [31] G. Colangelo, M. Hoferichter, and P. Stoffer, Two-pion contribution to hadronic vacuum polarization, *J. High Energy Phys.* **02** (2019) 006.
- [32] M. Hoferichter, B.-L. Hoid, and B. Kubis, Three-pion contribution to hadronic vacuum polarization, *J. High Energy Phys.* **08** (2019) 137.
- [33] M. Davier, A. Hoecker, B. Malaescu, and Z. Zhang, A new evaluation of the hadronic vacuum polarisation contributions to the muon anomalous magnetic moment and to $\alpha(m_Z^2)$, *Eur. Phys. J. C* **80**, 241 (2020); **80**, 410(E) (2020).
- [34] A. Keshavarzi, D. Nomura, and T. Teubner, The $g-2$ of charged leptons, $\alpha(M_Z^2)$ and the hyperfine splitting of muonium, *Phys. Rev. D* **101**, 014029 (2020).
- [35] A. Kurz, T. Liu, P. Marquard, and M. Steinhauser, Hadronic contribution to the muon anomalous magnetic moment to next-to-next-to-leading order, *Phys. Lett. B* **734**, 144 (2014).
- [36] K. Melnikov and A. Vainshtein, Hadronic light-by-light scattering contribution to the muon anomalous magnetic moment revisited, *Phys. Rev. D* **70**, 113006 (2004).
- [37] P. Masjuan and P. Sánchez-Puertas, Pseudoscalar-pole contribution to the $(g_\mu-2)$: A rational approach, *Phys. Rev. D* **95**, 054026 (2017).
- [38] G. Colangelo, M. Hoferichter, M. Procura, and P. Stoffer, Dispersion relation for hadronic light-by-light scattering: Two-pion contributions, *J. High Energy Phys.* **04** (2017) 161.
- [39] M. Hoferichter, B.-L. Hoid, B. Kubis, S. Leupold, and S. P. Schneider, Dispersion relation for hadronic light-by-light scattering: Pion pole, *J. High Energy Phys.* **10** (2018) 141.
- [40] A. Gérardin, H. B. Meyer, and A. Nyffeler, Lattice calculation of the pion transition form factor with $N_f = 2 + 1$ Wilson quarks, *Phys. Rev. D* **100**, 034520 (2019).
- [41] J. Bijnens, N. Hermansson-Truedsson, and A. Rodríguez-Sánchez, Short-distance constraints for the HLbL contribution to the muon anomalous magnetic moment, *Phys. Lett. B* **798**, 134994 (2019).
- [42] G. Colangelo, F. Hagelstein, M. Hoferichter, L. Laub, and P. Stoffer, Longitudinal short-distance constraints for the hadronic light-by-light contribution to $(g-2)_\mu$ with large- N_c Regge models, *J. High Energy Phys.* **03** (2020) 101.
- [43] T. Blum, N. Christ, M. Hayakawa, T. Izubuchi, L. Jin, C. Jung, and C. Lehner, Hadronic light-by-light scattering contribution to the muon anomalous magnetic moment from lattice QCD, *Phys. Rev. Lett.* **124**, 132002 (2020).
- [44] G. Colangelo, M. Hoferichter, A. Nyffeler, M. Passera, and P. Stoffer, Remarks on higher-order hadronic corrections to the muon $g-2$, *Phys. Lett. B* **735**, 90 (2014).
- [45] Sz. Borsanyi *et al.*, Leading hadronic contribution to the muon magnetic moment from lattice QCD, *Nature (London)* **593**, 51 (2021).
- [46] F. V. Ignatov *et al.* (CMD-3 Collaboration), Measurement of the $e^+e^- \rightarrow \pi^+\pi^-$ cross section from threshold to 1.2 GeV with the CMD-3 detector, [arXiv:2302.08834](https://arxiv.org/abs/2302.08834).
- [47] G. Colangelo *et al.*, Prospects for precise predictions of a_μ in the Standard Model, [arXiv:2203.15810](https://arxiv.org/abs/2203.15810).